Available online at www.sciencedirect.com
SCIENCE DIRECT®
Journal of Magnetic Resonance 168 (2004) 296–306
JMR Journal of Magnetic Resonance
www.elsevier.com/locate/jmr

A new sensitive isotropic–anisotropic separation experiment—SPEED MAS

Mark Strohmeier and David M. Grant*

Department of Chemistry, University of Utah, 315 S. 1400 E., Rm 2020, Salt Lake City, UT 84112-0850, USA

Received 8 October 2003
Available online 10 April 2004

Abstract

A new sensitive 2D isotropic–anisotropic separation experiment that utilizes stroboscopic phase encoding in the evolution dimension (SPEED) under magic angle sample spinning is presented. This 2D experiment consists of a train of $2N-1$ π pulses that are applied over $2N$ rotor periods. The π pulse train effectively reduces the apparent spinning speed in the evolution dimension by a factor of $1/(2N)$ from the mechanical spinning speed. Thus, problems commonly associated with magic angle turning such as stable slow spinning, different matching and TPPM proton decoupling conditions are avoided. Data replication similar to the five π replicated magic angle turning (FIREMAT) and pseudo 2D sideband suppression (P2DSS) experiments transfers resolution from the acquisition dimension to the evolution dimension. Hence, large spectral windows with good digital resolution are obtained with a few evolution increments. Here, slow spinning sideband patterns are extracted from the replicated 2D dataset with TIGER processing. Nevertheless, 2D Fourier transformation is also applicable. The extracted sideband patterns are identical to magic angle turning sideband pattern allowing for easy extraction of principal shift components. Accurate ^{13}C principal shift components are obtained for 3-methylglutaric acid using SPEED and FIREMAT experiments to validate the method. Furthermore, SPEED spectra for calcium acetate and α santonin are reported to show the wide applicability of this new experiment.

1. Introduction

During the last two decades, the chemical shift tensor has been recognized as a superb probe in many areas of chemistry and structural biology [1–3]. Several 2D techniques exist that measure the principal components of the shift tensor in powdered solids with dilute spin-1/2 systems such as ^{13}C, ^{15}N, ^{29}Si, and ^{31}P [4–8]. Many of these techniques utilize static or slow spinning (turning) samples that require special instrumentation for pulse synchronization, sample reorientation or slow spinning speeds that are difficult to maintain. In addition, Hartmann–Hahn [9,10] and ^{1}H TPPM [11,12] decoupling conditions are affected by the spinning speed and thus MAT experiments require a different experimental setup than commonly run high-speed MAS experiments. Nevertheless, MAT techniques are widely applied in many studies [13–17].

The above-mentioned difficulties can be avoided when anisotropic interactions are measured at high spinning speeds. Furthermore, such a ''recoupling'' sequence may easily be combined with other MAS sequences from the NMR spectroscopists' toolbox. However, only a few shift recoupling techniques have been published and have not yet gained wide popularity [18–21].

Here, we describe a new sensitive 2D isotropic–anisotropic separation experiment that encodes the isotropic shift information in the acquisition dimension and utilizes stroboscopic phase encoding in the evolution dimension (SPEED) to encode anistropic interactions corresponding to the various isotropic shifts in the evolution dimension. Both, sample replication [22] and sophisticated TIGER [23–25] processing are incorporated to increase the resolution in the evolution dimension and to extract phase sensitive sideband patterns from the phase encoded 2D dataset, respectively. The data replication allows for high-resolution and large spectral windows in the evolution dimension with only a few evolution increments. This is especially important

* Corresponding author. Fax: 1-801-581-8433.
E-mail address: grant@chem.utah.edu (D.M. Grant).

1090-7807/$ - see front matter © 2004 Elsevier Inc. All rights reserved.
doi:10.1016/j.jmr.2004.03.003

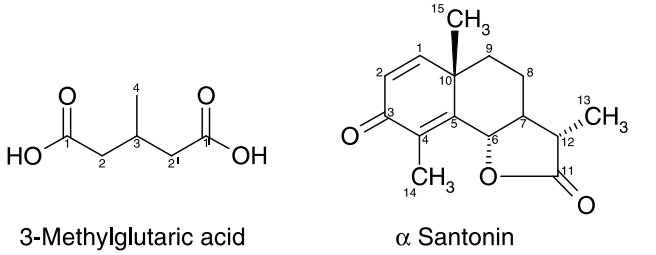

Fig. 1. Structures of 3-methylglutaric acid and α santonin. The carbon numbering is indicated.

when wide span tensors are measured with a limited number of evolution increments without sacrificing resolution and short experiment times. The experiment is a simple refocusing sequence with a train of π pulses timed to the rotor position; thus it is easy to implement on standard solid-state NMR spectrometer systems without the need for customized electronic hardware.

To validate the experiment, SPEED spectra for 3-methylglutaric acid (see Fig. 1) with different SPEED sequences are obtained and the extracted ^{13}C principal shift components are compared to values measured with the FIREMAT technique. In addition, SPEED spectra for calcium acetate and α santonin (see Fig. 1) are reported to show the wide applicability of this new experiment to larger more relevant compounds.

2. Theory

The basic idea of this constant time experiment is based on sidebands at half the mechanical spinning speed in the evolution dimension of FIREMAT experiments that appear for higher-order interactions [26]. Thus, many ideas from this powerful MAT experiment such as data replication and TIGER processing are easily incorporated. The pulse sequence consists of $N-1$ π pulses that are applied at even rotor periods and N π pulses removed from odd rotor periods with a time τ as shown in Fig. 2A. The precession of the complex magnetization M_+ is encoded in the evolution dimension by the stroboscopic timing of the π pulses. The integer number N specifies the factor by which the effective mechanical spinning speed ω_r is reduced in the evolution dimension.

The evolution of the magnetization for a crystallite ρ_{2D} created by such a sequence may be expressed by

$$\rho_{2D}(\alpha,\beta,\gamma|\tau,t_2) = \exp[-i\Phi(\alpha,\beta,\gamma|\tau)]\cdot\sum_k a_k(\alpha,\beta,\gamma) \cdot \exp[-i(W_0(\alpha,\beta)+k\omega_r)t_2], \quad (1)$$

where $\Phi(\alpha,\beta,\gamma|\tau)$ represents the phase angle accumulated during the evolution period. The angles α, β, and γ represent the orientation of the Zeeman field and the rotor axis in a crystallite or molecular fixed frame as

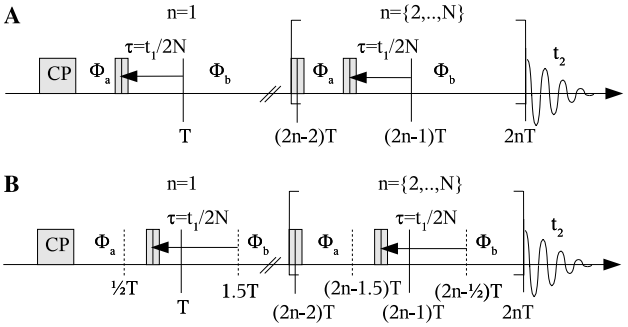

Fig. 2. Pulse sequence of the: (A) basic and (B) symmetrized SPEED MAS experiment.

specified in Fig. 3. Relaxation is omitted for the description of the experiment, but will be discussed later. The right-hand side of Eq. (1) represents the free precession of a rotating crystallite in the acquisition dimension with sidebands at multiples of the spinning speed ω_r from the isotropic frequency W_0 that have complex amplitude a_k. Sufficient high spinning speeds or stroboscopic acquisition remove the sidebands in the acquisition dimension and thus Eq. (1) may be simplified to:

$$\rho_{2D}(\alpha,\beta,\gamma|\tau,t_2) = \exp[-i\Phi(\alpha,\beta,\gamma|\tau.)]\cdot\exp[-iW_0(\alpha,\beta)t_2]. \quad (2)$$

The phase angle accumulated by the train of π pulses is given by the sum of phase angles Φ_a and Φ_b accumulated in the repeating two rotor periods of the sequence. The second phase Φ_b is defined to be positive and Φ_a is negative since π pulses reverse the sign of the phase angles. The moving and fixed π pulses are always

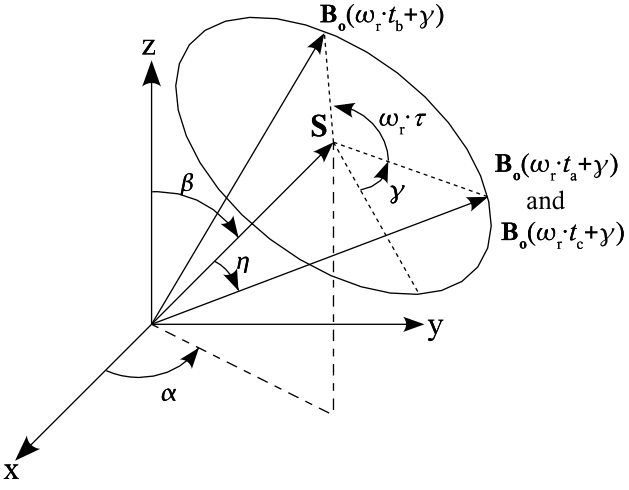

Fig. 3. Orientation of the sample rotor axis **S** and the Zeeman field $\mathbf{B}_0$ in a molecular or crystallite frame. η designates the magic angle. The times t_a and t_c are integer multiples of the rotor period T as given in Eq. (5), i.e., the $\mathbf{B}_0$ always has the same orientation in the crystallite frame when pulses are applied at t_a and t_c. The orientation of $\mathbf{B}_0(\omega_r\cdot t_b+\gamma)$ when the moving pulses are applied, progresses through the γ circle with increasing τ.

applied at the same rotor position during the sequence so that the phase angle Φ_n for the repeating part of the sequence is identical, i.e.,

$$\Phi_n(\alpha,\beta,\gamma|\tau) = \Phi_{n+1}(\alpha,\beta,\gamma|\tau). \tag{3}$$

Hence, following sum for the phase angle accumulated during the evolution period is obtained:

$$\Phi(\alpha,\beta,\gamma|\tau) = \sum_{n=1}^{N}(\Phi_b(\alpha,\beta,\gamma|\tau) - \Phi_a(\alpha,\beta,\gamma|\tau))_n. \tag{4}$$

The phase angle accumulated between pulses may be described as the time integral of the frequency function ω that is defined by the anisotropic interactions present in the solid. The boundaries of the integrals are defined by the times t_a, t_b, and t_c when pulses are applied.

$$\Phi(\alpha,\beta,\gamma|\tau) = \sum_{n=1}^{N}\left(\int_{t_b}^{t_c}\omega(\alpha,\beta,\gamma|\tau)\,\mathrm{d}t - \int_{t_a}^{t_b}\omega(\alpha,\beta,\gamma|\tau)\,\mathrm{d}\tau\right)_n,$$

$$\text{where } t_a = (2n-2)T,\ t_b = (2n-1)T-\tau \text{ and } t_c = 2nT. \tag{5}$$

The frequency function ω can be described by a Fourier series around the γ circle.

$$\omega(\alpha,\beta,\gamma|t) = \sum_{m=-\infty}^{\infty} W_m(\alpha,\beta)\cdot\exp[\mathrm{i}m\gamma]\cdot\exp[\mathrm{i}m\omega_r t]. \tag{6}$$

Analytical expressions for the expansion coefficients W_m are easily obtained from standard spin quantum mechanics [27]. For the most common interactions in dilute spin systems such as the chemical shift and heteronuclear dipolar coupling to spin 1/2 the series terminates at $m = \pm 2$. However, for other interactions such as the dipolar coupling to a quadrupolar nucleus (e.g., ^{35}Cl and ^{37}Cl) higher order coefficients exist for $|m| > 2$ and may become appreciable [26,27].

Using the symmetry of the frequency function $\omega(\alpha,\beta,\gamma|\tau)$ i.e.,

$$\int_{t_b}^{t_c}\omega(\alpha,\beta,\gamma|\tau)\,\mathrm{d}\tau = -\int_{t_a}^{t_b}\omega(\alpha,\beta,\gamma|\tau)\,\mathrm{d}\tau. \tag{7}$$

Eq. (5) may be simplified to

$$\Phi(\alpha,\beta,\gamma|\tau) = 2N\left(\int_{t_b}^{t_a}\omega(\alpha,\beta,\gamma|\tau)\,\mathrm{d}\tau\right). \tag{8}$$

Solving the integral in Eq. (8) yields for the phase angle accumulated during the evolution period:

$$\Phi(\alpha,\beta,\gamma|\tau) = 2NW_0\tau + \sum_{m=-\infty}^{\infty}\mathrm{i}\frac{2NW_m\exp[\mathrm{i}m\gamma]}{m\omega_r}\cdot(\exp[\mathrm{i}m\omega_r\tau]-1). \tag{9}$$

The phase angle for the free precession of a spin in a rotating crystallite is described by

$$\Phi_{\mathrm{free}}(\alpha,\beta,\gamma|t) = \int_0^t\omega(\alpha,\beta,\gamma|\tau)\,\mathrm{d}\tau, \tag{10}$$

and after solving the integral one obtains

$$\Phi_{\mathrm{free}}(\alpha,\beta,\gamma|t) = W_0 t + \sum_{m=-\infty}^{\infty}\mathrm{i}\frac{W_m\exp[\mathrm{i}m\gamma]}{m\omega_r}(\exp[\mathrm{i}m\omega_r t]-1). \tag{11}$$

By comparison of Eqs. (10) and (11) and defining $\tau = t_1/2N$ it is obvious that the apparent spinning speed in the indirect dimension of the SPEED experiment is $\omega_{\mathrm{app}} = \omega_r/2N$. Thus, the FID obtained in the evolution dimension of the SPEED sequence is equivalent to a FID at a lower spinning speed with the same sideband amplitudes.

Hence, the resulting SPEED evolution FID may be expressed as a set of frequencies (sidebands) with complex amplitudes $a_k(\alpha,\beta,\gamma)$, spaced by ω_{app} and centered around the isotropic frequency $W_0(\alpha,\beta)$.

$$\exp\left[-\mathrm{i}W_0 t_1 - \mathrm{i}\sum_{m=-\infty}^{\infty}\mathrm{i}\frac{W_m(\alpha,\beta)\exp[\mathrm{i}m\gamma]}{m\omega_{\mathrm{app}}}\cdot(\exp[\mathrm{i}m\omega_{\mathrm{app}}t_1]-1)\right] = \sum_k a_k(\alpha,\beta,\gamma)\cdot\exp[-\mathrm{i}(W_0(\alpha,\beta)+k\omega_{\mathrm{app}})t_1]. \tag{12}$$

The sideband amplitudes $a_k(\alpha,\beta,\gamma)$ may be computed from the Fourier coefficients $W_m(\alpha,\beta)$ using the banded matrix approach [27]. The complete 2D FID for the SPEED experiment may then be written as:

$$\rho_{2D}(\alpha,\beta,\gamma|t_1,t_2) = \left(\sum_k a_k(\alpha,\beta,\gamma)\cdot\exp[-\mathrm{i}(W_0(\alpha,\beta)+k\omega_{\mathrm{app}})t_1]\right)\cdot\exp[-\mathrm{i}W_0(\alpha,\beta)t_2]. \tag{13}$$

For most common interaction such as the chemical shift and heteronuclear dipolar coupling to a spin-1/2 in dilute spin systems, W_0 is independent of crystallite orientation and the Fourier expansion terminates at $m = \pm 2$. After integration over the powder angles, the evolution of the complex magnetization M_+ may be expressed as:

$$M_+(t_1,t_2) = M_0\left(\sum_k A_k\cdot\exp[-\mathrm{i}(W_0+k\omega_{\mathrm{app}})t_1]\right)\cdot\exp[-\mathrm{i}W_0 t_2], \tag{14}$$

where A_k is the real amplitude of the observed sidebands and M_0 is the initial magnetization after cross polarization.

3. Replication

The pulse sequence allows acquisition of only $\tau = (t_1/2N) < T$ and thus limits the maximum resolution in the evolution dimension to the apparent spinning speed ω_{app}. Replication is utilized in order to increase the resolution far beyond this limitation. Eq. (14) shows that:

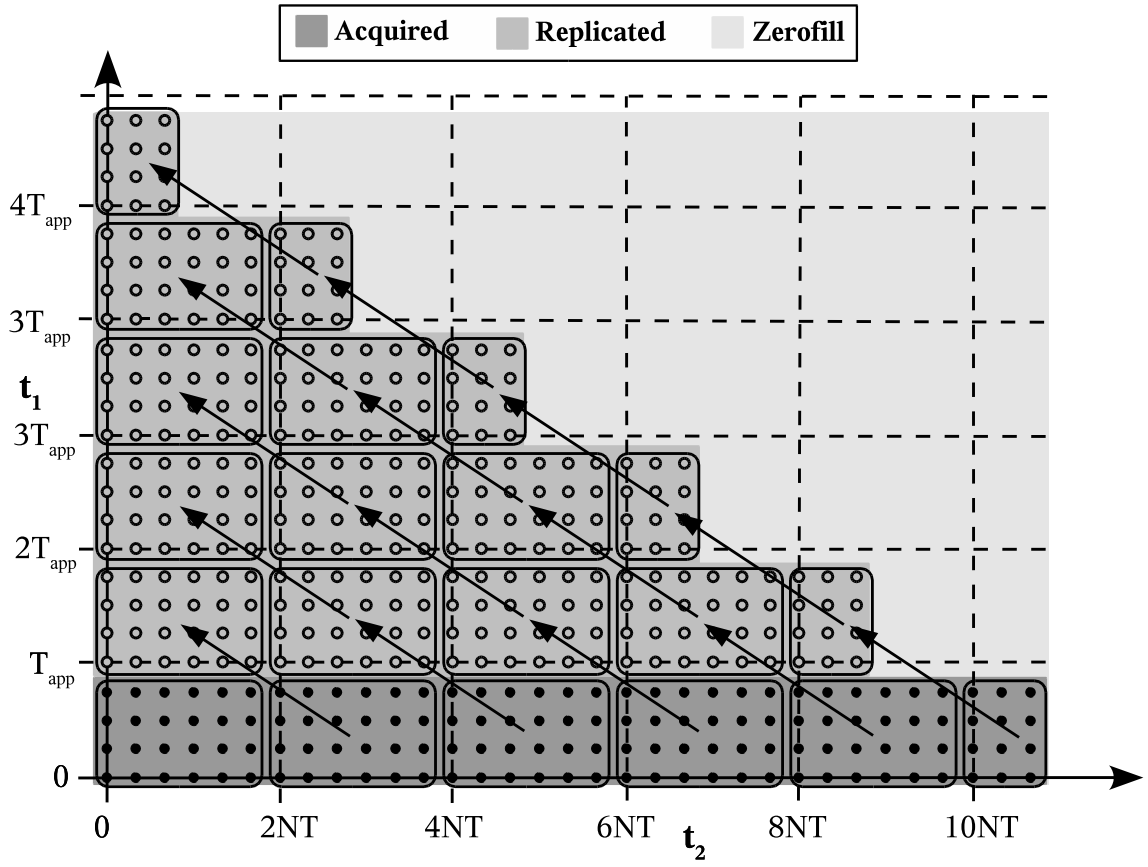

Fig. 4. Replication scheme applied to create the full SPEED FID.

$$M_+(t_1, t_2 + nT_{\text{app}}) = M_+(t_1 + nT_{\text{app}}, t_2),$$
$$\text{where } T_{\text{app}} = \frac{1}{\omega_{\text{app}}}. \tag{15}$$

When the evolution and acquisition dimensions are sampled with dwell times (dw) that are an integer fraction of the apparent spinning speed, the replication scheme shown in Fig. 4 can be applied effectively to increase the maximum evolution time. This allows for a large spectral window with a digital resolution equal to the acquisition dimension to accommodate tensors with large spans without sacrificing resolution. In many other experiments, where anisotropic information is encoded in the evolution dimension, many evolution increments must be taken in order to accommodate large tensor spans with acceptable resolution. The replication is similar to the replication in the FIREMAT [6] and P2DSS [22] experiments. In all cases it is used to increase the limited resolution in an evolution dimension.

4. Symmetry of the sequence

Pulse collisions in the pulse sequence at high spinning speeds and large spectral windows in the evolution dimension may occur when the π pulse width is longer than $\tau = \text{dw}_1/2N$. This can be avoided when the sequence is symmetrized by acquiring evolution increments for $t_1 = -T_{\text{app}}/2$ to $t_1 < T_{\text{app}}/2$ as depicted in Fig. 2B. This avoids pulse collisions, but introduces a first order phase shift in the evolution dimension of the SPEED FID as follows:

$$M_+(t_1, t_2) = M_0\left(\sum_k A_k \cdot \exp[-\mathrm{i}(W_0 + k\omega_{\text{app}}) \cdot \left(t_1 - \tfrac{1}{2}T_{\text{app}}\right)]\right) \cdot \exp[-\mathrm{i}W_0 t_2]. \tag{16}$$

Rearranging yields

$$M_+(t_1, t_2) = M_0\left(\sum_k A_k \cdot \exp[-\mathrm{i}(W_0 + k\omega_{\text{app}})t_1 + \mathrm{i}W_0\tfrac{1}{2}T_{\text{app}} + \mathrm{i}k\pi]\right) \cdot \exp[-\mathrm{i}W_0 t_2]. \tag{17}$$

With the first order phase shift for a sideband pattern divided into $W_0 T_{\text{app}}/2 = \xi$ and the real factor $\exp[\mathrm{i}k\pi] = (-1)^k$ one obtains:

$$M_+(t_1, t_2) = M_0\left(\sum_k (-1)^k A_k \cdot \exp[-\mathrm{i}(W_0 + k\omega_{\text{app}})t_1 + \xi]\right) \cdot \exp[-\mathrm{i}W_0 t_2]. \tag{18}$$

When the centerband of an extracted sideband pattern is zero-order phase corrected by ξ then all sidebands are in phase, but have alternating amplitudes in accordance with Eq. (18). Symmetrizing the pulse sequence also reduces artifacts from non-refocusable line broadening as will be shown in the next section. Fig. 5 shows sideband pattern for C1 and C2 carbon positions in 3-methylglutaric acid extracted from experiments with a different experimental number N, generating different apparent spinning speeds. The number of evolution in-

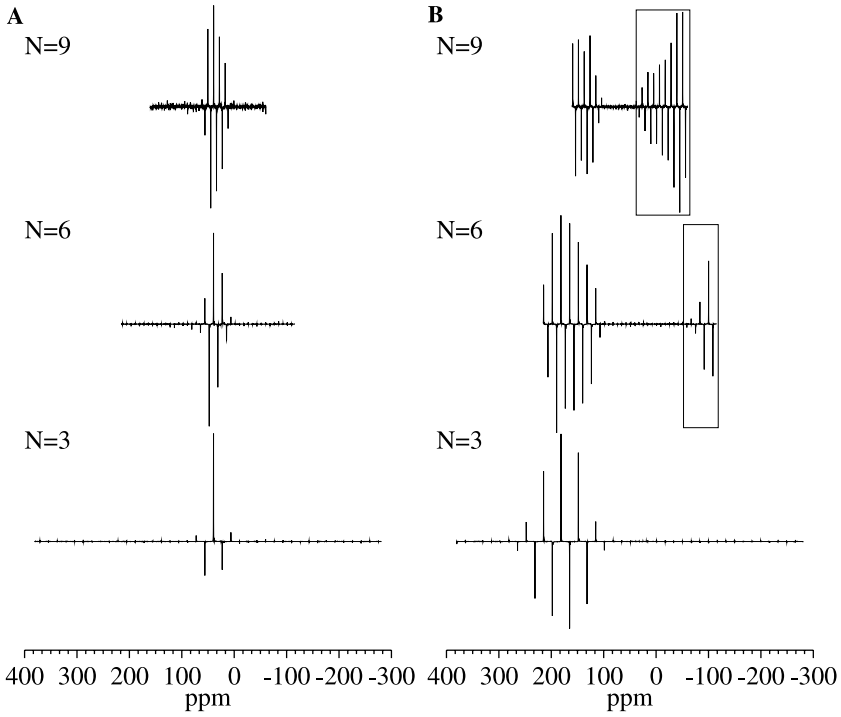

Fig. 5. (A) C2 and (B) C1 sideband pattern of 3-methylglutaric acid extracted from SPEED spectra with 40 evolution increments. The mechanical spinning speed was 5 kHz for all experiments. Hence, corresponding apparent spinning speeds are 833.33, 416.67, and 277.78 Hz for $N = 3$, $N = 6$, and $N = 9$, respectively. Sidebands in boxed areas are aliased from higher frequencies.

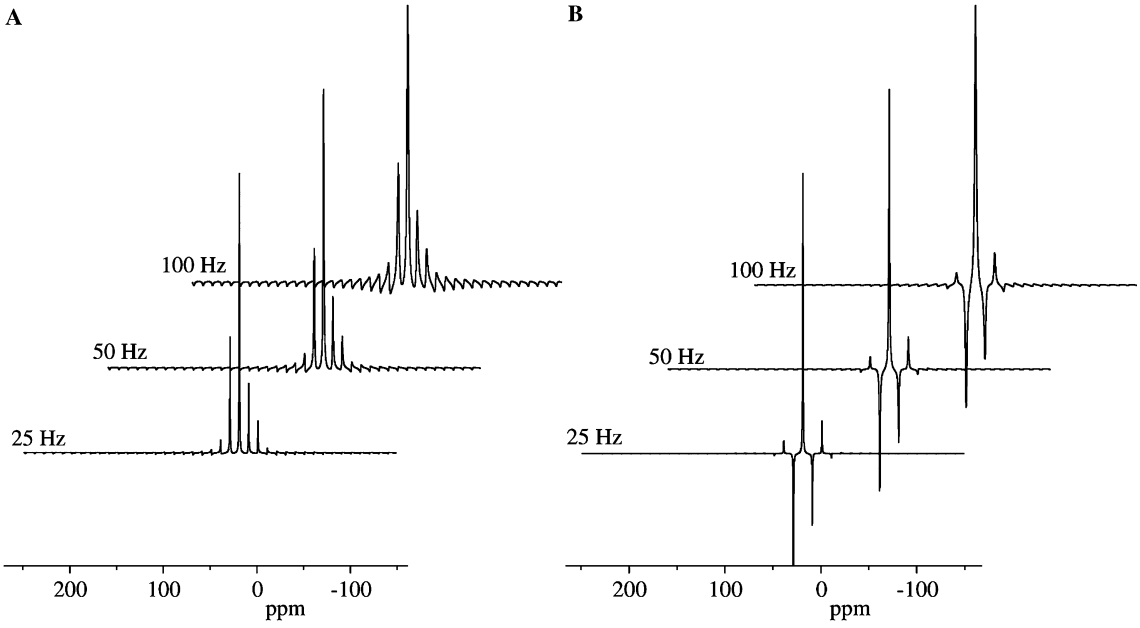

Fig. 6. Simulation of relaxation artifacts caused by non-refocusable linebrodening. (A) Basic pulse sequence. (B) Symmetrized pulse sequence. Non-refocussable line widths are given next to the simulations.

crements and the mechanical spinning speed was kept constant. This figure shows the alternating amplitudes of the sidebands in the symmetrized pulse sequence even at low apparent spinning speeds. Furthermore, it reveals that aliasing of sidebands may be used efficiently to choose apparent spinning speed, spectral window, and number of increments in the evolution dimension that would accommodate wide and narrow tensor spans simultaneously. In Fig. 5 for example the number of sidebands with significant amplitude, i.e., the information content, is increased just by changing the experimental number N, not by increasing the number of increments in the evolution dimension.

5. Relaxation

During the acquisition period the detectable magnetization decays with a specific time constant T_2. The interactions leading to the decay of the magnetization may be divided into two groups, with π pulses refocusable and non-refocusable. Non-refocusable interactions, designated by the specific time constant T_2^*, are small in most compounds. For example for several natural abundance ^{13}C samples natural line widths of about 0.5–10 Hz are reported even without TPPM decoupling [28]. However, non-refocusable line broadening may become considerably large in systems with molecular motion,

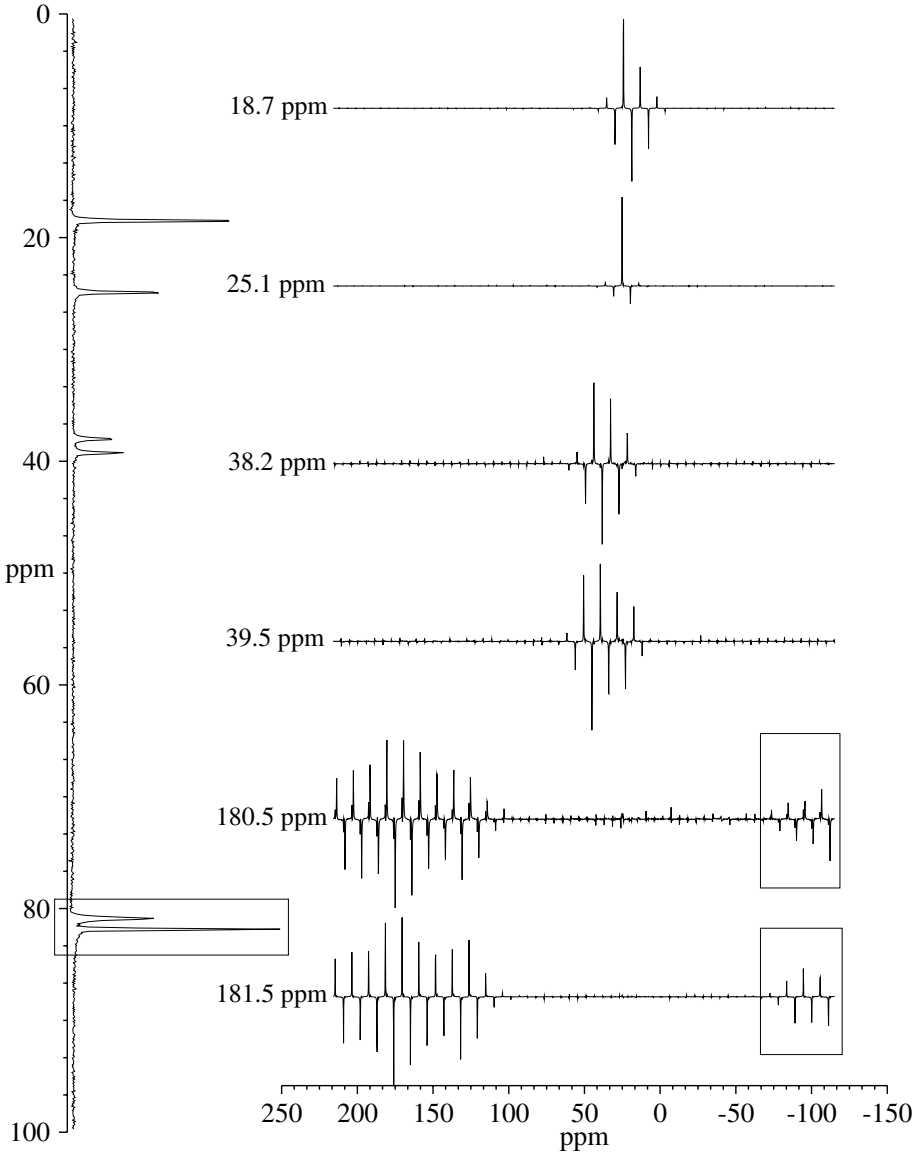

Fig. 7. Replicated and TIGER processed SPEED spectrum of 3-methylglutaric acid. The mechanical spinning speed was 5 kHz and $N = 9$ with 60 increments in the evolution dimension. The spectral windows were 5 and 16.667 kHz in the acquisition and evolution dimension, respectively. The repetition time was 3 s and 144 transients were accumulated per increment. The guide spectrum is shown on the left and the extracted spectra are shown on the right-hand side. Numbers on the sideband patterns indicate the isotropic shift. Resonances in boxed areas are aliased from higher frequencies.

insufficient proton decoupling and enriched samples with considerable homonuclear dipolar coupling. Since non-refocusable interactions dephase the magnetization during the evolution period regardless of the refocusing pulse position τ, they do not contribute to the evolution dimensions decay function. Hence, non-refocusable interactions only result in a reduced sensitivity.

The difference in decay constants between evolution and acquisition dimension results in steps in the decay function of the evolution dimension when replication is applied to the 2D dataset [6]. The complete 2D FID including relaxation may thus be written as:

$$M_+(t_1,t_2) = M_0\left(\sum_k A_k \cdot \exp[-\mathrm{i}(W_0 + k\omega_{\mathrm{app}})t_1]\right) \cdot \exp\left[-\frac{t_1}{T_2 - T_2^*}\right] \cdot \exp\left[-\frac{T_{\mathrm{app}}}{T_2^*}\left(\mathrm{int}\left(\frac{t_1}{T_{\mathrm{app}}}\right)+1\right)\right] \cdot \exp[-\mathrm{i}W_0 t_2] \cdot \exp[-t_2/T_2]. \quad (19)$$

Since the steps in the decay function occur at multiples of the apparent rotor period T_{app}, sideband artifacts appear for each sideband pattern at frequencies separated by the apparent spinning speed ω_{app} as shown in Fig. 6. For a regular sideband pattern these artifacts accumulate and may affect the spectrum considerably, especially when $1/T_2^*$ becomes large, as demonstrated in Fig. 6A. However, the symmetrized sequence yields sidebands with alternating amplitudes, hence the relaxation artifacts for the alternating sidebands cancel even for large $1/T_2^*$ as observed in Fig. 6B.

6. TIGER and absolute value mode Fourier transformation

Ideally TIGER processing is used to extract phase sensitive sideband patterns for individual isotropic carbon positions. The high-resolution guide spectrum needed for the TIGER procedure is directly obtained from the increment with $t_1 = 0$ of the 2D dataset. Figs. 7–9 show examples of TIGER extracted sideband pattern for 3-methylglutamic acid, α santonin, and calcium acetate, respectively. In the example compounds sideband patterns for isotropic shifts as close as 0.2 ppm are resolved in calcium acetate and as may as 28 shift pattern are extracted for α santonin. Hence, the SPEED experiment may be used to investigate even larger systems when sufficient resolution in the acquisition dimension is present. Principal components of the chemical shift tensor and/or heteronuclear dipolar coupling tensors are easily extracted from the individual sideband pattern by nonlinear fitting with an appropriate model. TIGER may also accommodate small sidebands in the guide spectrum that result from insufficient spinning speed.

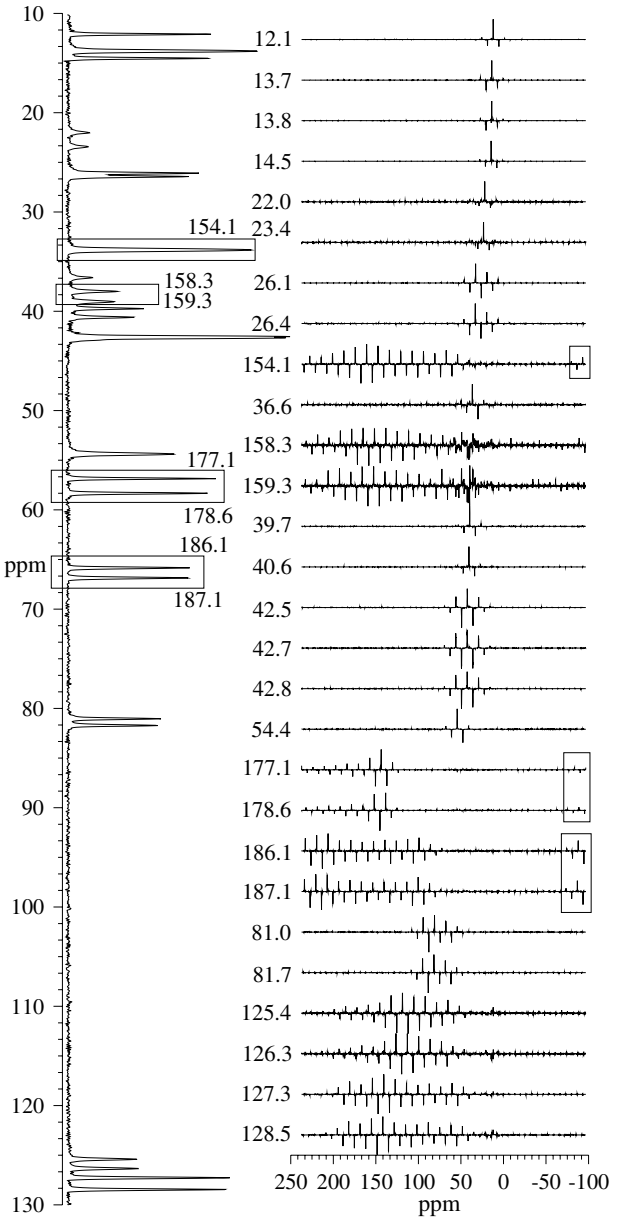

Fig. 8. Replicated and TIGER processed santonin SPEED experiment. The mechanical spinning speed was 6 kHz and $N = 9$ with 50 increments in the evolution dimension. The spectral windows were 6 and 16.667 kHz in the acquisition and evolution dimension, respectively. The repetition time was 3 s and 432 were accumulated transients per increment. The guide spectrum is shown on the left and the extracted spectra are shown on the right-hand side. Numbers on the sideband patterns indicate the isotropic shift in ppm. Resonances in boxed areas are aliased from higher frequencies. The isotropic shifts in ppm of the aliased resonances in the guide spectrum are indicated. For many positions in α santonin the two molecules per asymmetric unit are resolved.

Alternatively, absolute value Fourier transformation may be used to display the complete SPEED spectrum in a sensible way and may also be used to extract individual absolute value sideband pattern as depicted in Figs. 10 and 11. Some of the problems associated with the display of the large dynamic range of absolute value SPEED spectra are revealed in Fig. 10, i.e., some of the sideband

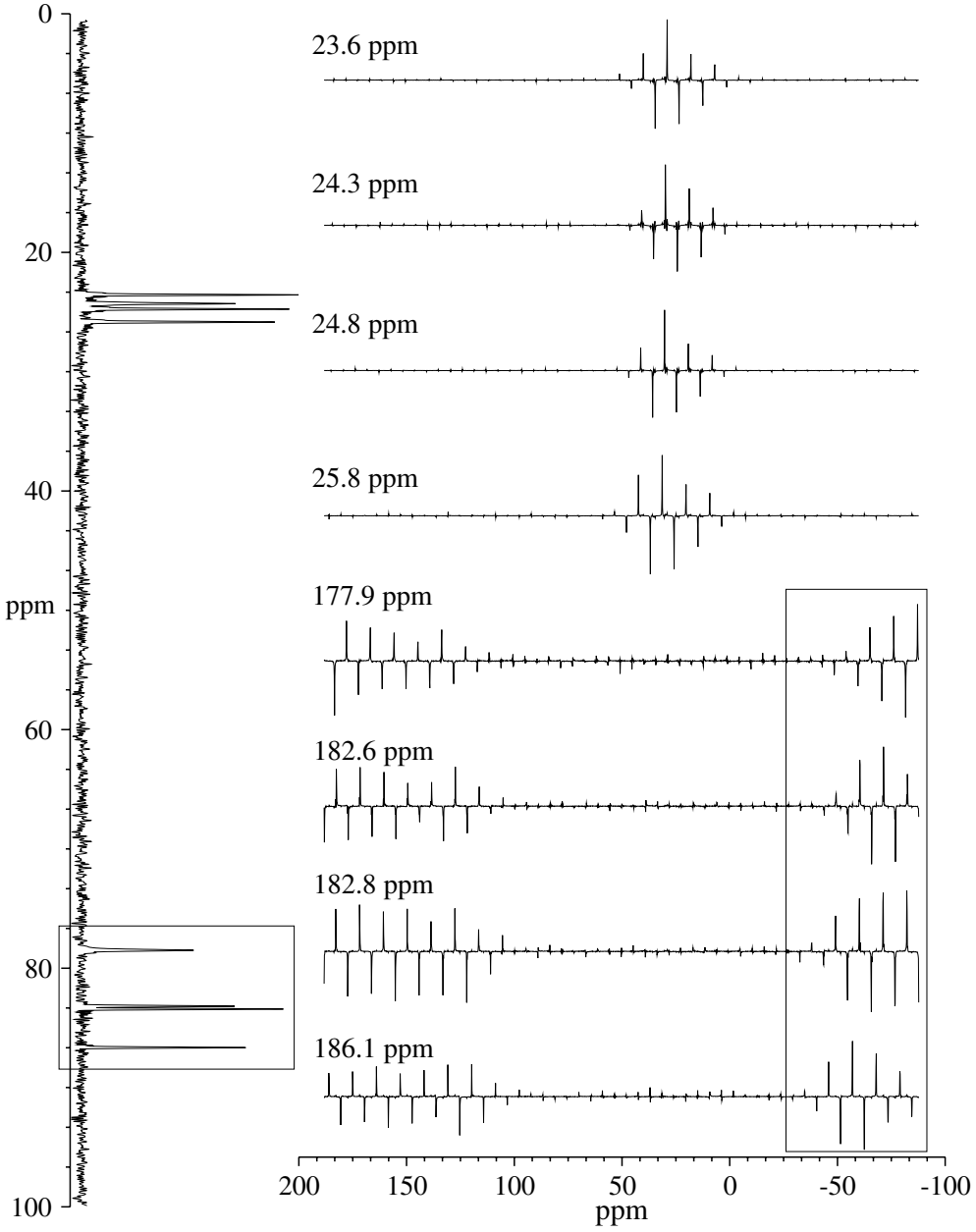

Fig. 9. Replicated and TIGER processed calcium acetate SPEED experiment. The down field carboxylate resonances are aliased in the guide spectrum. The mechanical spinning speed was 5 kHz and $N = 9$ with 50 increments in the evolution dimension. The spectral windows were 6 and 13.889 kHz in the acquisition and evolution dimension, respectively. The repetition time was 9 s and 144 transients were accumulated per increment. The guide spectrum is shown on the left and the extracted spectra are shown on the right-hand side. Numbers on the sideband patterns indicate the isotropic shift. Resonances in boxed areas are aliased from higher frequencies. All four acetate molecules per asymmetric unit are resolved for both methyl and carboxylate carbons. Sideband patterns for isotropic positions as as close as 0.2 ppm (10 Hz) are resolved.

patterns are absent in the display. This results primarily from large sideband amplitudes in high intensity narrow span sideband pattern and small amplitude sidebands in low intensity wide span sideband pattern.

7. Phase cycling

The phase cycling for the experiments with $N = 3$ is taken from the FIREMAT experiment [6]. In sequences with $N > 3$, the $2N - 1$ π pulses in the pulse sequence are divided into two groups: moving and fixed π pulses. The phases of the moving pulses are increased from the first having 0° by 360° /N to the last moving π pulse in the sequence having (360–360/N)° The phases of the fixed pulses are increased similarly by 360°/($N - 1$). The phase cycling for the following transients with number i is then performed by propagating the phase angle of 360°/($N + i$) for the moving pulses and 360°/($N - 1 + i$) for the fixed pulses, respectively. Fig. 12 gives a

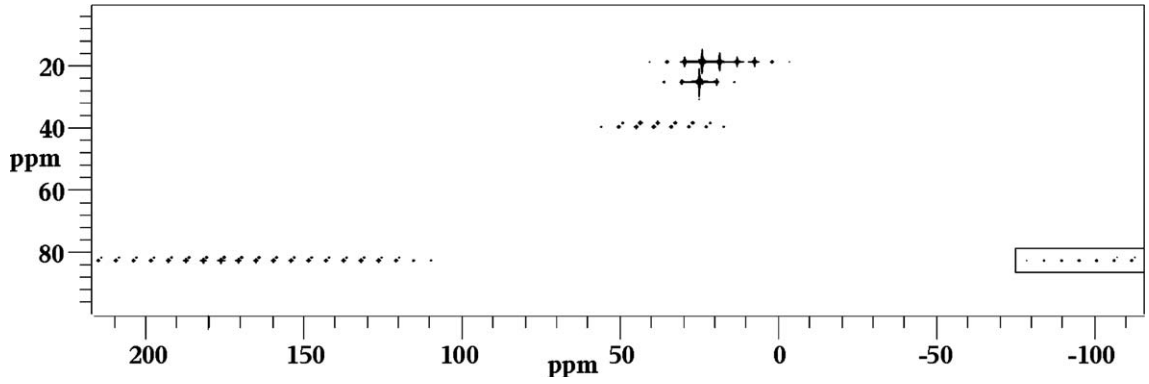

Fig. 10. Replicated and absolute value Fourier transformed SPEED spectrum of 3-methylglutamic acid. The same dataset as in Fig. 7 is shown. Aliased sidebands are enclosed by boxes. Both C1 and C1′ sideband pattern appearing at 81 and 81.5 ppm in the isotropic dimension are also aliased in the acquisition dimension from 180.0 and181.5 ppm, respectively.

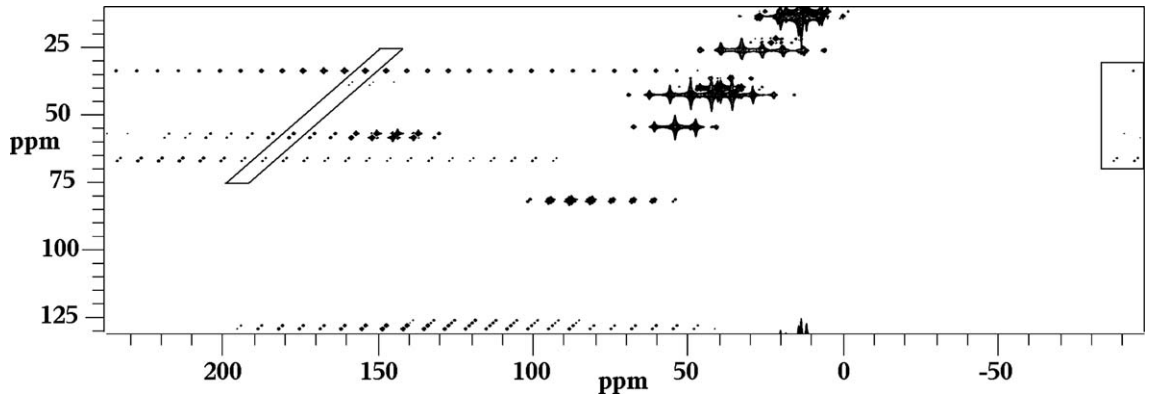

Fig. 11. Absolute Value FT spectrum of the santonin SPEED experiment. The same dataset as in Fig. 8 is shown. Aliased sidebands are enclosed in a square box. The centerbands of sideband pattern aliased in the acquisition dimension are enclosed in a parallelogram.

graphical representation of the phase cycling for $N = 6$. It was found that it is not necessary to permute through all phase combinations possible, presumably because the pulse sequence including the rotor position is repetitive after every two-rotor period. A standard four-cycle CYCLOPS sequence is included to remove carrier and receiver artifacts [29]. Hence, a relatively short phase cycle, i.e., the smallest common multiplier of 4, N and $(N-1)$, is obtained. This change allows for SPEED sequences with large N without inhibitive lengthening the phase cycling. The phase cycle may be dramatically decreased utilizing cogwheel phase cycling proposed by Levitt et al. [30]. This is under further investigation for trains of refocusing pulses used in various experiments.

8. Validation of the method

To validate the method, shift tensors extracted from several SPEED MAS experiments are compared to the corresponding FIREMAT data using the root-mean-squared (rms) distance between tensors. Tables 1 and 2 summarize the SPEED and FIREMAT extracted icosahedral shift components [31] and lists the rms distances for the corresponding tensors. The agreement between the FIREMAT data and the SPEED data is excellent and combined results for all positions in 3-methylglutamic acid range from 1.5 ppm for the SPEED experiment with $N = 6$ and 40 evolution increments to 1.7 ppm for the SPEED experiment with $N = 3$ and 40 evolution increments. These values are comparable to intrinsic experimental measurement errors of both approaches and establish the reliability of the SPEED method. The intrinsic error of the SPEED experiment may be further reduced by experimental improvements such as synchronization of pulse timing and acquisition to the rotor position utilizing a feedback circuit. This may become necessary at higher spinning speeds or less stable spinning conditions.

9. Experimental

All experiments were performed on a Chemagnetics CMX200 spectrometer operating at 50.306 MHz ^{13}C frequency and equipped with a 7.5 mm Pencil rotor probe. TPPM proton decoupling was used in all exper-

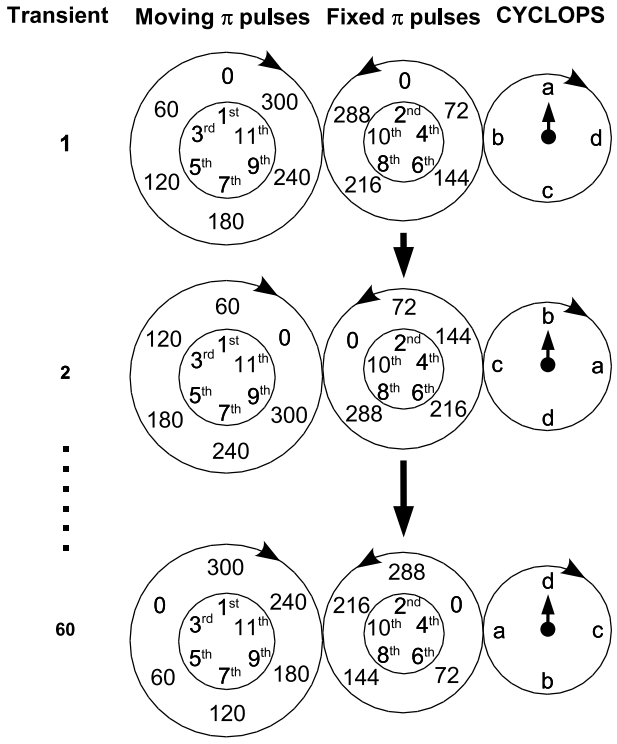

Fig. 12. Dials describing the phase cycling for a SPEED sequence with $N = 6$. The four cycles of CYCLOPS are designated from a to c. The inner "hubs" of the dials give the π pulse number in the sequence. The phase of the pulses are given in degrees on the propagating dials.

iments with a phase shift angle of 14° at high spinning speeds and 32° in the MAT experiments. The π pulse lengths for ^{13}C and ^{1}H were between 8 and 9 μs in all experiments. Carbon magnetization was produced using standard cross polarization. The spinning speed was controlled to approximately ±2 Hz using the standard Chemagnetics spin controller software.

For replication it is required that the acquisition spectral width for SPEED experiments is a multiple of the mechanical spinning speed ensuring digitization of the signal at the rotor echo. The acquisition is done stroboscopically, i.e., the spectral window equals the spinning speed, so that sidebands are absent in the acquisition dimension. The synchronization of pulse timing and acquisition using a feedback circuit was omitted for all SPEED experiments, but will increase the accuracy of the experiment. A feedback synchronization might become necessary at larger spinning speeds, larger N or for less stable spinning conditions.

FIREMAT spectra were recorded at a mechanical spinning speed of 300 and 500 Hz. The spectral windows were 9.6 and 8.0 kHz in the evolution dimension and 57.600 and 48.077 kHz in the acquisition dimension, 32 and 16 evolution increments were taken at 300 and 500 Hz spinning speed, respectively. The acquisition and the pulse timing in the FIREMAT experiments were synchronized to the rotor position using a feedback circuit [4]. Phase sensitive sideband patterns for individual isotropic shifts were extracted from the FIREMAT spectra using TIGER processing.

Table 1
Icosahedral shift components of 3-methylglutamic acid in ppm extracted from SPEED spectra [32]

	δ_a	δ_c	δ_e	δ_{avg}	rmsd[b]
SPEED 9_60[a]					
C1	234.0	158.6	151.8	181.5	1.0
C1′	235.2	154.9	151.4	180.5	0.5
C2	56.4	34.1	28.0	39.5	2.6
C2′	53.0	33.5	28.3	38.3	1.5
C4	30.5	21.6	23.3	25.1	1.7
C3	29.3	17.7	9.2	18.7	0.5
SPEED 9_40[a]					
C1	234.1	158.3	151.5	181.3	0.9
C1′	233.8	155.0	152.2	180.3	1.4
C2	56.3	33.7	27.9	39.3	2.7
C2′	52.7	33.1	28.3	38.1	1.6
C4	30.2	20.5	24.2	25.0	2.2
C3	29.0	17.5	9.2	18.5	0.5
SPEED 6_40[a]					
C1	233.9	158.6	152.0	181.5	1.2
C1′	234.1	156.2	151.2	180.5	1.5
C2	57.1	35.4	26.0	39.5	1.2
C2′	53.2	33.9	27.6	38.2	1.0
C4	31.6	20.8	23.1	25.2	2.5
C3	26.8	23.0	6.5	18.7	0.8
SPEED 3_40[a]					
C1	234.6	158.9	151.0	181.5	0.5
C1′	233.0	157.9	150.7	180.5	2.7
C2	57.9	35.9	24.7	39.5	0.7
C2′	53.4	35.0	26.4	38.2	0.5
C4	29.8	25.9	19.7	25.1	2.5
C3	28.6	20.4	7.2	18.7	1.6

[a] The first number corresponds to N, the second to the number of evolution increments in the experiment.
[b] Root-mean-squared distance to the FIREMAT 300 shift tensor.

Table 2
Icosahedral shift components of 3-methylglutamic acid in ppm extracted from FIREMAT spectra [32]

	δ_a	δ_c	δ_e	δ_{avg}	rmsd[b]
FIREMAT 300[a]					
C1	235.2	158.7	150.5	181.5	—
C1′	235.9	154.3	151.3	180.5	—
C2	57.1	36.7	24.4	39.4	—
C2′	52.6	35.3	26.6	38.2	—
C4	28.4	23.7	23.2	25.1	—
C3	28.8	18.3	8.9	18.7	—
FIREMAT 500[a]					
C1	235.0	159.1	150.9	181.6	0.4
C1′	235.5	154.9	151.5	180.7	0.4
C2	56.2	37.7	24.2	39.4	0.8
C2′	52.1	36.0	26.3	38.1	0.6
C4	28.2	24.2	22.6	25.0	0.5
C3	28.8	18.3	8.7	18.6	0.1

[a] Spinning speed in Hz used in the experiment.
[b] Root-mean-squared distance to the FIREMAT 300 shift tensor.

3-Methylglutamic acid and α santonin were obtained from Aldrich and used as received. Calcium acetate was recrystallized from water.

10. Conclusion

We are reporting a new isotropic–anisotropic separation MAS experiment that utilizes stroboscopic phase encoding in the evolution dimension (SPEED). Replication is used to increase the resolution in the evolution dimension to minimize the number of increments needed to determine the anisotropic information in the evolution dimension. Furthermore, efficient TIGER processing is implemented to extract sideband patterns for individual isotropic positions. The method is validated by comparison of shift tensors obtained for 3-methylglutamic acid with this new experiment and the well-established FIREMAT technique and good agreement is found. In addition, spectra of α santonin and calcium acetate are presented to show the wide applicability of the experiment.

Acknowledgments

This work benefited greatly from insightful discussions with D.W. Alderman. Jim K. Harper is thanked for suggesting α santonin as an example compound as well as for preparing the calcium acetate sample. Funding for this research was provided by NIH under Grant GM 08521-41 and DOE under Grant DE FG 03-94ER 14452.

References

[1] D.M. Grant, in: D.M. Grant, R.K. Harris (Eds.), Encyclopedia of NMR, vol. 2, Wiley, Chichester, 1996, pp. 1298–1321.
[2] D.A. Case, Curr. Opin. Struct. Biol. 8 (1998) 624–630.
[3] P.A. Tishmack, D.E. Bugay, S.R. Byrn, J. Pharm. Sci 92 (2003).
[4] A. Bax, N.M. Szeverenyi, G.E. Maciel, J. Magn. Reson. 52 (1982) 147.
[5] J.Z. Hu, D.W. Alderman, C. Ye, R.J. Pugmuire, D.M. Grant, J. Magn. Reson. A 105 (1993) 82.
[6] D.W. Alderman, G. McGeorge, J.Z. Hu, R.J. Pugmuire, D.M. Grant, Mol. Phys. 95 (1998) 1113, and references therein.
[7] O.N. Antzukin, S.C. Shekar, M.H. Levitt, J. Magn. Reson. 115 (1995) 7.
[8] A.M. Orendt, in: D.M. Grant, R.K. Harris (Eds.), Encyclopedia of NMR, vol. 2, Wiley, Chichester, 1996, pp. 1282–1297.
[9] A. Pines, M.G. Gibby, J.S. Waugh, J. Chem. Phys. 59 (1973) 569–590.
[10] E.O. Stejksdal, J. Schaefer, J.S. Waugh, J. Magn. Reson. 28 (1977) 105–112.
[11] A.E. Bennet, C.M. Rienstra, M. Auger, K.V. Lakshmi, R.G. Griffin, J. Chem. Phys. 103 (1995) 6951.
[12] G. McGeorge, D.W. Alderman, D.M. Grant, J. Magn. Reson. 137 (1999) 138.
[13] M. Strohmeier, A.M. Orendt, D.W. Alderman, D.M. Grant, J. Am. Chem. Soc. 123 (2001) 1713–1722.
[14] Y. Wei, D.-K. Lee, A. Ramamoorthy, J. Am. Chem Soc. 123 (2001) 6118–6126.
[15] D.-K. Lee, Y. Wei, A. Ramamoorthy, J. Phys. Chem. B 105 (2001) 4752–4762.
[16] X. Yao, M. Hong, J. Am. Chem Soc. 124 (2002) 2730–2738.
[17] J.K. Harper, G. McGeorge, D.M. Grant, J. Am. Chem. Soc. 121 (1999) 6488–6496.
[18] R. Tycko, G. Dabbagh, P.A. Mirau, J. Magn. Reson. 85 (1989) 265.
[19] S.-F. Liu, J.-D. Mao, K. Schmidt-Rohr, J. Magn. Reson. 155 (2002) 15–28.
[20] B. Elena, S. Hediger, L. Emsley, J. Magn. Reson. 160 (2003) 40–46.
[21] C. Crockford, H. Geen, J.J. Titman, Chem. Phys. Lett. 344 (2001) 367–373.
[22] Z. Gan, J. Magn. Reson. A 109 (1994) 253.
[23] Y. Manassen, G. Navon, C.T.W. Moonen, J. Magn. Reson. 72 (1987) 551.
[24] Y. Manasen, G. Navon, J. Magn. Reson. 79 (1988) 291.
[25] G. McGeorge, J.Z. Hu, C.L. Mayne, D.W. Alderman, R.J. Pugmire, D.M. Grant, J. Magn. Reson. 129 (1997) 134.
[26] M. Strohmeier, D.W. Alderman, D.M. Grant, J. Magn. Reson. 155 (2002) 263–277.
[27] N.K. Sethi, D.W. Alderman, D.M. Grant, Mol. Phys. 71 (1990) 217.
[28] Y.J. Jiang, R.J. Pugmuire, D.M. Grant, J. Magn. Reson. 71 (1987) 485.
[29] D.J. Hoult, R.E. Richards, Proc. Roy. Soc. (London) A 344 (1975) 311.
[30] M.H. Levitt, P.K. Madhu, C.E. Hughes, J. Magn. Reson 155 (2002) 300–306.
[31] D.W. Alderman, M.H. Sherwood, D.M. Grant, J. Magn. Reson. A 101 (1993) 188.
[32] In the original paper, introducing the icosahedral representation of second rank tensors, the components were numbered from one to six. Here, the icosahedral components are designated from a to f in order to avoid confusion with the convention of the Cartesian numbering of the principal components.